



Article

Novel Nano-Therapeutic Approach Actively Targets Human Ovarian Cancer Stem Cells after Xenograft into Nude Mice

Amoura Abou-ElNaga ¹, Ghada Mutawa ¹, Ibrahim M. El-Sherbiny ², Hassan Abd-ElGhaffar ³, Ahmed A. Allam ^{4,5}, Jamaan Ajarem ⁴ and Shaker A. Mousa ^{6,*}

¹ Zoology Department, Faculty of Sciences, Mansoura University, Mansoura 35516, Egypt; dramabouelnaga@yahoo.com (A.A.-E.); ghada.adel.mutawa@gmail.com (G.M.)

² Center for Materials Science, Zewail City of Science and Technology, Cairo 12588, Egypt; ielsherbiny@zewailcity.edu.eg

³ Clinical Pathology Department, Faculty of Medicine, Mansoura University, Mansoura 35516, Egypt; Haabdelghaffar@yahoo.com

⁴ Zoology Department, College of Science, King Saud University, Riyadh 11451, Saudi Arabia; aallam@ksu.edu.sa (A.A.A.); jajarem@ksu.edu.sa (J.A.)

⁵ Zoology Department, Faculty of Science, Beni-Suef University, Beni-Suef 62511, Egypt

⁶ The Pharmaceutical Research Institute, Albany College of Pharmacy and Health Sciences, Rensselaer, NY 12144, USA

* Correspondence: shaker.mousa@acphs.edu; Tel.: +1-518-694-7397

Academic Editor: Yogesh Kumar Vashist

Received: 7 February 2017; Accepted: 24 March 2017; Published: 12 April 2017

Abstract: The power of tumorigenesis, chemo-resistance and metastasis in malignant ovarian tumors resides in a tiny population of cancer cells known as ovarian cancer stem cells (OCSCs). Developing nano-therapeutic targeting of OCSCs is considered a great challenge. The potential use of poly(lactic-co-glycolic acid) nanoparticles (PLGA NPs) was investigated as a drug delivery system for paclitaxel (PTX) against OCSCs in vitro and in vivo. PTX-loaded PLGA NPs were prepared by an emulsion solvent evaporation method, supported by incorporation of folic acid (FA) as the ligand. NPs were characterized for size, surface morphology, drug loading, and encapsulation efficiency. In vitro cytotoxicity of PTX-loaded FA/PLGA NPs was tested against OCSCs with MTT assay. In vivo anti-tumoral efficiency and active targeting potential of prepared NPs against tumors in nude mice were investigated. In vitro results revealed that IC₅₀ of PTX was significantly reduced after loading on PLGA NPs. On the other hand, in vivo results showed that PLGA NPs enhanced the tumor suppression efficiency of PTX. Investigation with real time quantitative PCR analysis revealed the limiting expression of chemo-resistant genes (*ABCG2* and *MDR1*) after applying PLGA NPs as a drug delivery system for PTX. Histopathological examination of tumors showed the effective biological influence of PTX-loaded FA/PLGA NPs through the appearance of reactive lymphoid follicles. Targeting potential of PTX was activated by FA/PLGA NPs through significant preservation of body weight ($p < 0.0001$) and minimizing the systemic toxicity in healthy tissues. Immunohistochemical investigation revealed a high expression of apoptotic markers in tumor tissue, supporting the targeting effect of FA/PLGA NPs. A drug delivery system based on FA/PLGA NPs can enhance PTX's in vitro cytotoxicity and in vivo targeting potential against OCSCs.

Keywords: PLGA; drug delivery system; paclitaxel; ovarian cancer stem cells; nude mice

1. Introduction

Ovarian cancer is one of the most lethal types of gynecologic malignancy [1]. Ovarian cancer stem cells (OCSCs) are a small subpopulation of ovarian cancer cells that are capable of self-renewal and differentiation into multiple ovarian malignant cell types. The ovarian cancer cells that express CD44+ exhibit cancer stem cell-like properties of migration and chemo-resistance. CD44+ phenotype cells within ovarian tumors correlate to the risk of cancer relapse and metastasis [2].

Paclitaxel (PTX) is a standard chemo-drug against ovarian tumors. Improving an appropriate vehicle system for PTX has proven to be difficult due to its chemical properties of hydrophobicity and insolubility. Additionally, the commercial form of PTX is far from perfect due to toxicity of the carriers, such as Cremophor-EL [3]. The other obstacle in ovarian cancer therapy is the difficulty of targeting the CSCs' subpopulation in ovarian tumors using traditional drug carriers [4]. CSCs stimulate effective chemo-drug resistance pathways that pump the toxic drugs out of the cells [5]. Due to the presence of efflux mechanisms, by increasing expression of defense factors involved in reducing intra-cellular drug dose such as ATP binding cassette (ABC) and multi-drug resistance (MDR) transporters, CSCs are resistant to the current chemotherapy compared to non-tumorigenic cells [6]. Nanotechnology may represent a promising drug delivery system (DDS) that can safely target OCSCs within malignant ovarian tumors [7].

Progress in nanotechnology and medicine has led to the development of many nano-structural materials for therapeutic applications. Nanoscale DDS based on polymeric particles has been the subject of intensive research due to their high therapeutic effect against cancers. Nanoparticles (NPs) provide many unique advantages that are not available with other traditional cancer therapies [8].

NPs made from biodegradable polymers have attracted great interest for targeting cancer cells with reduced systemic side effects [9]. Poly(lactic-co-glycolic acid) (PLGA) is a successful biodegradable polymer because it hydrolyzes into two monomers: lactic acid and glycolic acid. Both monomers are metabolized through the Krebs cycle. Reduction of drug side effects is correlated to the application of PLGA as the DDS [10]. PLGA has attractive properties as a chemo-drug carrier; the European Medicine Agency and the US Food and Drug Administration approved PLGA as an ideal DDS because of its biocompatibility and biodegradability. PLGA synthesis can be adapted to hydrophilic and hydrophobic drugs, thus avoiding degradation of the drug, and it provides sustained release and the possibility to target specific tissues or cells [11].

NPs can target cancers by both active and passive mechanisms. Passive targeting uses the property of the nano-scaled size of polymeric particles and exploits the abnormal structure and architecture of the tumor's blood vessels. NPs pass through the discontinuous endothelial cells and aggregate inside the interstitial spaces between the tumor cells. This is termed "enhanced permeability". In addition, tumors' cells have ineffective lymphatic vessels, which cause insufficient drainage of cancer cells. This is termed "enhanced retention". Both phenomena are called the enhanced permeability and retention effect. This effect is considered as a gold standard in the synthesis of new anti-cancer DDS [12].

Targeting mechanisms are activated by ligands that are grafted on the surface of NPs [11]. The ligand is chosen to bind specific receptors overexpressed by tumor cells or tumor vasculature but not by normal cells. The expression of the targeted receptor on all cancer cells is considered to be an important factor in determining the needed ligand. The enhanced cellular uptake is important for effective anti-cancer therapy through actively targeted nano-deliveries [13]. Targeting cancer cells can be achieved through the highly expressed receptors, such as the folate receptor (FR). FR is a highly-selective tumor marker over-expressed in many human cancers such as ovarian tumors. Because folic acid (FA) expression is limited in healthy tissues and organs, FR is considered to be a main target for cancer-specific chemo-drug carriers. Thus, the incorporation of FA in drug carriers enhances the delivery of these drugs to FR-positive tumor cells [14].

In this study, PLGA NPs were synthesized, loaded with PTX, and incorporated with FA. Size, surface morphology, drug loading, and encapsulation efficiency of the resultant PTX-FA/PLGA NPs were characterized. In addition, the *in vitro* antineoplastic efficiency and *in vivo* targeting efficiency

of PTX-FA/PLGA NPs against OCSCs were also investigated. Here, we focused on the pathological evaluation of the PLGA NPs' targeting and therapeutic effect against tumor tissue, specifically the CSC subpopulation, through histopathological examination, immunohistochemical investigation, and molecular analysis. We also evaluated the new DDS for targeting OCSCs instead of tumor bulk.

2. Results

2.1. Characteristics of PTX-Loaded FA/PLGA NPs

The mean diameter of PTX-loaded FA/PLGA NPs was 294.7 nm (Figure 1a). Data from SEM showed the NPs as singular and non-aggregated particles, with a smooth surface morphology (Figure 1b). TEM data showed the NPs distributed as individual particles with clear spherical shape and dispersed homogeneously with a size of 100–200 nm (Figure 1c). Drug loading and encapsulation efficiency were calculated to be 1.46% and 73%, respectively.

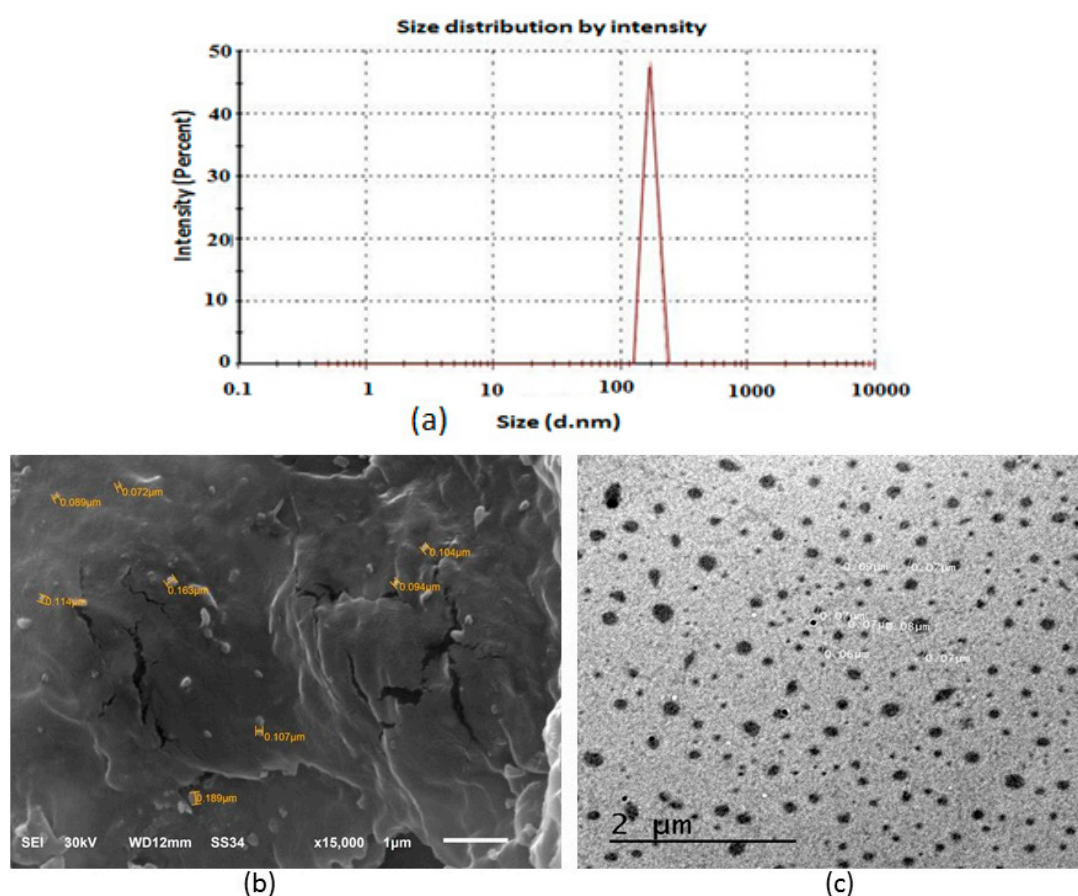


Figure 1. Characteristics of PTX-loaded FA/PLGA NPs. (a) Size distribution measured with photon correlation spectroscopy using a Zetasizer; (b) SEM image; (c) TEM image.

2.2. In Vitro Antineoplastic Efficiency of PTX-Loaded FA/PLGA NPs

The in vitro antineoplastic efficiency of free PTX and PTX-loaded FA/PLGA NPs against OCSCs after 24 h was evaluated with the MTT assay (Figure 2a,b). Results showed that the PTX-loaded FA/PLGA NPs had more antineoplastic efficiency than free PTX for OCSCs at all different doses (0.5–10 nM), while free PTX IC_{50} was 2.49-fold greater than PTX-loaded FA/PLGA NPs IC_{50} .

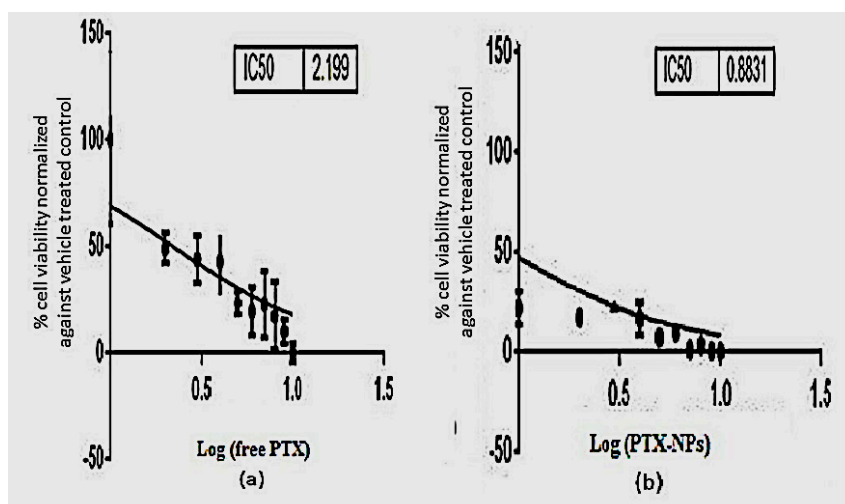


Figure 2. Antineoplastic efficiency of PTX-loaded FA/PLGA NPs on OCSCs in vitro. (a) Cytotoxicity of free PTX and (b) PTX-loaded FA/PLGA NPs against OCSCs after 24 h. IC₅₀ of PTX-loaded FA/PLGA NPs was 0.8831 nM and, of free PTX, was 2.199 nM.

2.3. In Vivo Targeting Efficiency of PTX-Loaded FA/PLGA NPs

2.3.1. Tumor Volume and Body Weight Change after Treatment

Tumor suppressing efficiency 5 days after injection of samples was visually detected (Figure 3a). Obvious palpable tumors in xenograft mice were observed after injection of saline and plain NPs. There was visually clear suppression of tumors in xenograft mice after injection of free PTX. In contrast, tumors in xenograft mice disappeared after injection of PTX-loaded FA/PLGA NPs.

Change in tumor volume after treatment was detected daily (Figure 3b); the first day of sample injection was day 0 (tumor volume = 1125 mm³). There was no significant change in tumor volume from injection with plain NPs as compared with saline ($p = 0.78$). There was significant suppression of tumor volume in treated groups (free PTX and PTX-loaded NPs) when compared with control group (saline), which continued its ascending growth ($p < 0.0001$). In contrast, tumor volume in PTX-loaded NPs injected mice was non-significantly suppressed when compared with tumor volume of free PTX injected mice at the end of treatment (0.56 and 74 mm³, respectively, $p = 0.22$).

Variation of body weight after treatment was detected daily (Figure 3c). Significant body weight loss in treated mice was observed after treatment with free PTX and PTX-loaded NPs when compared with control group, which was injected with saline ($p < 0.0001$). In contrast, the body weight of free PTX injected mice was significantly lower than that of PTX-loaded NPs injected mice at the end of treatment (18.2 and 20 g, respectively, $p < 0.0001$).

2.3.2. Histopathological Examination of Tumor and Main Organ Sections

Sections of adjacent areas of excised tumors after formalin fixation and paraffin embedding and histopathological examination are shown in Figure 4a. Aggregates of spindle shaped cells clearly appeared (arrow) in sections of control tumors that were injected with saline and plain NPs. We noted disappearance of spindle shaped cells in sections of free PTX treated tumors. On the other hand, reactive lymphatic follicles appeared (arrow) in sections of tiny nodules that remained in the skin at the site of injection of PTX-loaded NPs.

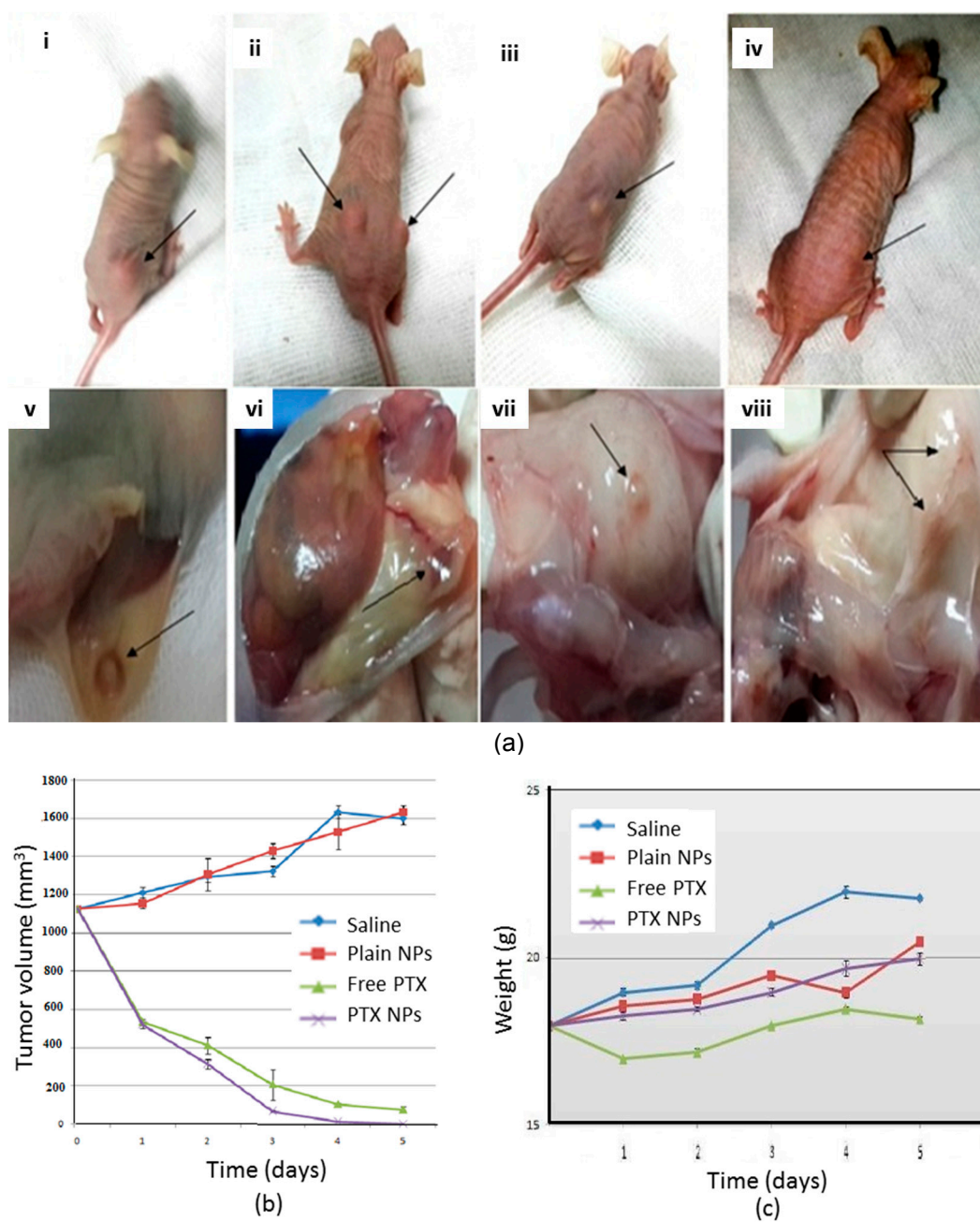


Figure 3. Targeting efficiency of PTX-loaded FA/PLGA NPs in vivo. (a) Visual tumor size change at the end of treatment; (b) Tumor volume change after treatment; (c) Mice body weight change after treatment. In (a), external views: (i) saline; (ii) plain NPs; (iii) free PTX; (iv) PTX-loaded FA/PLGA NPs. Internal views: (v) saline; (vi) plain NPs; (vii) free PTX; (viii) PTX-loaded FA/PLGA NPs. In (a), arrows in (i,v) and (ii,vi) point to obvious appearance of tumors, (iii,vii) to visual clear suppression of tumors, and (iv,viii) to tumor disappearance.

Sections of the main organs showed no clear pathological variation between groups except intestine (Figure 4b). We noted clear rupture of intestine (arrow) in the case of free PTX treated mice, whereas intestine section of PTX-loaded NPs treated mice were absolutely free of any damage when compared to control.

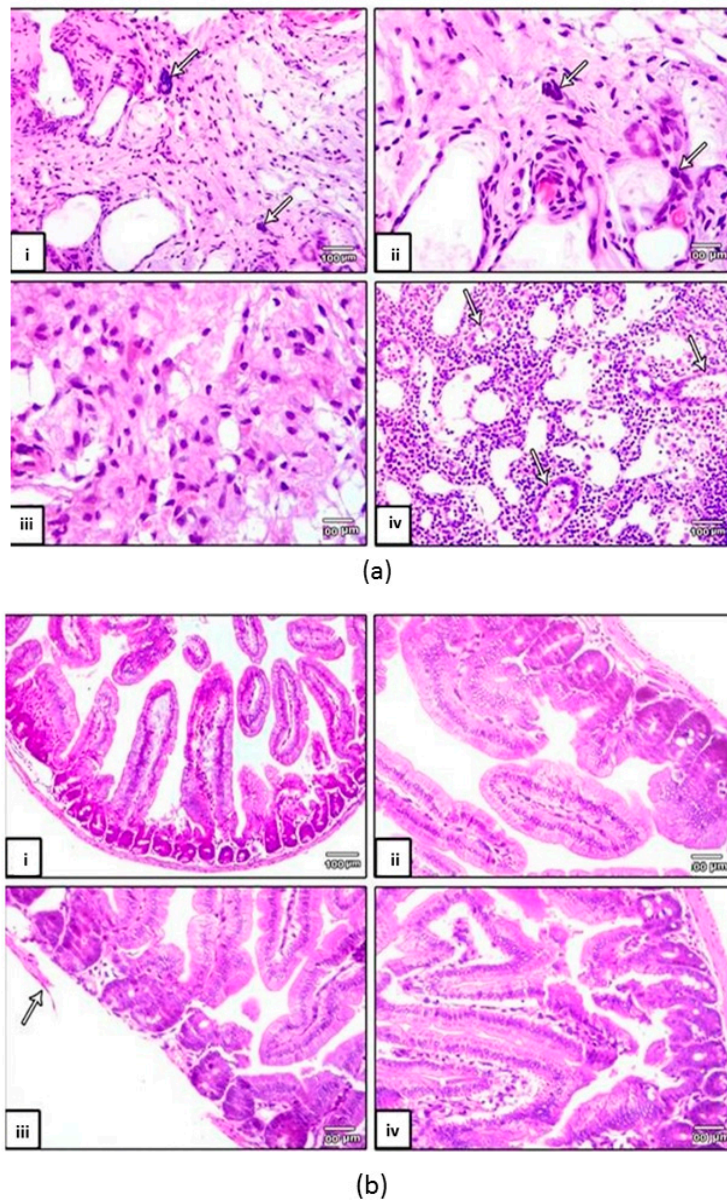


Figure 4. Histopathological examination. (a) Tumor sections and (b) intestine after the treatments (H&E staining): (i) saline; (ii) plain NPs; (iii) free PTX; (iv) PTX-loaded FA/PLGA NPs. In (a), arrows in (i,ii) point to aggregates of cancer cells and in (iv) to reactive lymphoid follicles; In (b), the arrow in (iii) points to a clear rupture in intestinal serosa.

2.3.3. Immunohistochemical Examination of Apoptotic and Tumor Suppressor Proteins

Expressions of caspase-3 as apoptotic marker and P53 as tumor suppressor protein were detected with immunohistochemistry (Figure 5a,b, respectively). Immunohistochemical staining showed brown color for positive expression, mainly located in the cell membrane and the cytoplasm of tumor cells; the positive expression exhibited diffuse or focal distribution. We noted high expressions of caspase-3 and P53 for free PTX and PTX-loaded NPs when compared with saline and plain NPs. Results showed intensive caspase-3 and P53 expressions in the PTX-loaded NPs group.

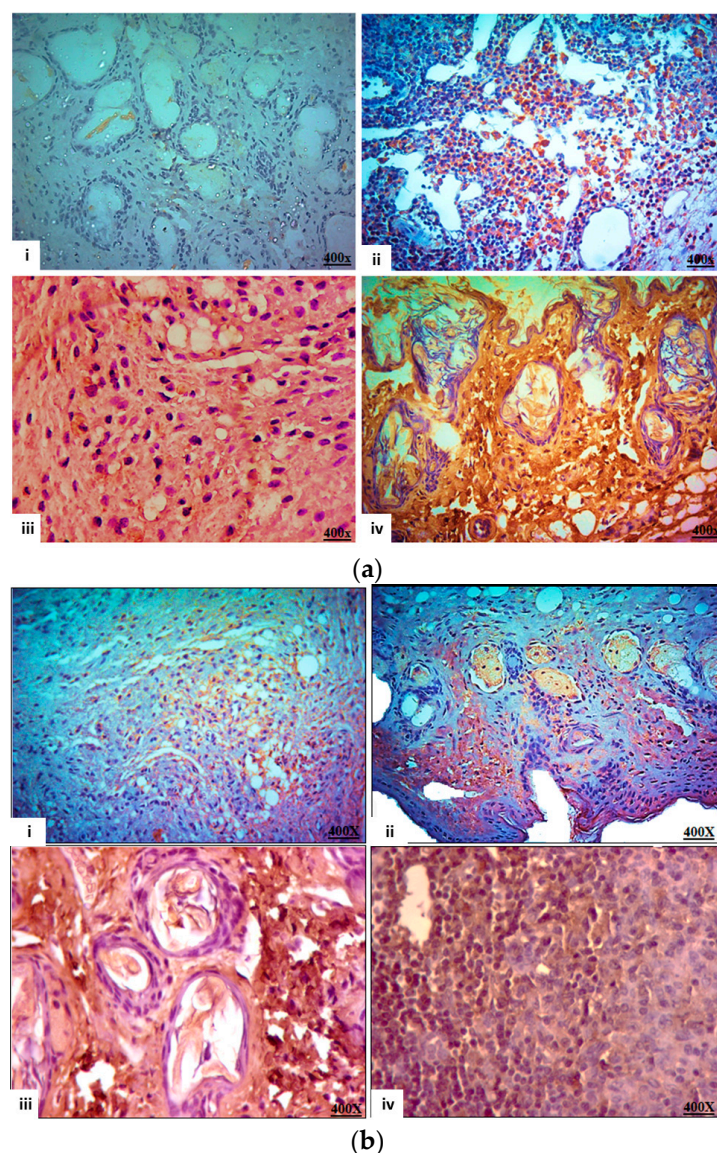


Figure 5. Immunohistochemistry. Expression of (a) *Caspase-3* and (b) *P53* in tumor tissues after the treatments (400×). (i) saline, (ii) plain NPs, (iii) free PTX, (iv) PTX-loaded FA/PLGA NPs.

2.3.4. mRNA Expression of Apoptotic, Chemo-Resistant and Tumor Suppressor Genes

RT-qPCR analysis was applied to detect the expression of apoptosis-related cysteine peptidase-9 (*caspase9*), apoptosis-related cysteine peptidase-3 (*caspase3*), tumor suppressor 53 (*TP53*), ATP-binding cassette sub-family G-2 (*ABCG2*) and multidrug resistance-1 (*MDR1*) in tumor sections treated with PTX-loaded NPs in comparison with free PTX (Figure 6a,b). Results showed no clear variation in the expressions of apoptotic genes (*caspase9* and *caspase3*) and tumor suppressor gene (*TP53*) between tumors treated with PTX-loaded NPs and free PTX, while PTX-loaded NPs expressed these genes 0.8-fold, two-fold, and four-fold, respectively, when compared with that of free PTX. Additionally, PTX expressed chemo-resistant genes (*ABCG2* and *MDR1*) 256-fold and 512-fold, respectively, greater than PTX after incorporation into FA/PLGA NPs.

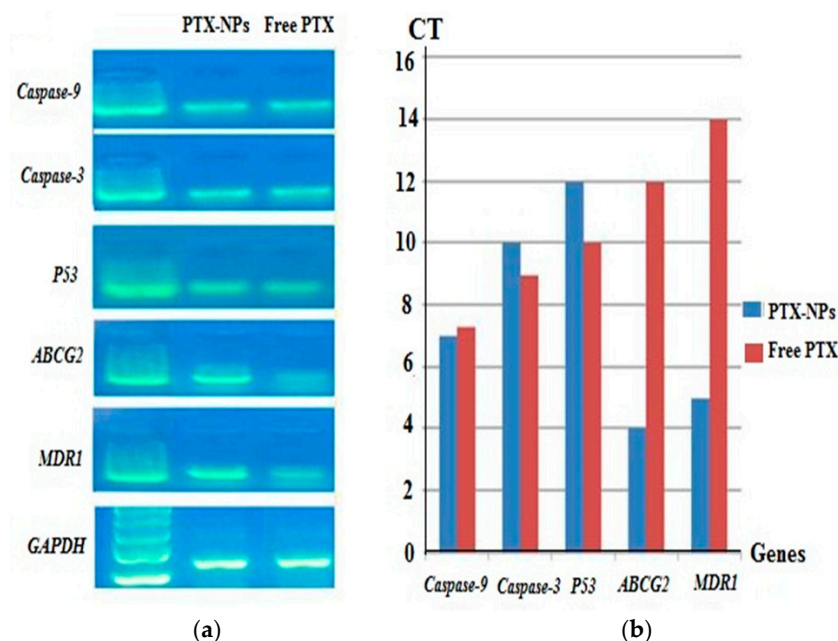


Figure 6. Expression of *caspase9*, *caspase3*, *TP53*, *ABCG2*, and *MDR1* mRNA. (a) PCR analysis and (b) RT-qPCR analysis. Lane 1: PTX-loaded FA/PLGA NPs treated tumors, Lane 2: free PTX. *GAPDH* was used as an internal control.

3. Discussion

We have recently published on the establishment and characterization of primary human OCSCs^{CD44⁺ve}, which have implications in ovarian cancer relapse and metastasis [15]. The novelty of the present study is the ability of FA/PLGA NPs in targeting and treating cancer stem cells (CSCs), especially in ovarian cancer. A major challenge here is overcoming the unique properties of CSCs' subpopulation within ovarian solid tumor, particularly the chemo-resistance property. As previously reported, an effective cancer treatment has to not only destroy cancer cells that represent the bulk of tumor cell population but also destroy CSCs [16]. PLGA has previously been applied as an ideal DDS in cancer treatment [11], so in our study we used PLGA as an effective carrier polymer for PTX to OCSCs with an activating targeting mechanism of grafting FA as a ligand to recognize FR-expressed ovarian cancer cells.

Pharmaceutical scientists are using NPs to minimize toxicity and side effects of chemo-drugs, although NPs themselves may cause hazards to the biological system. The risks of using NPs as DDS have previously been shown to be related to the chemical reagents used in the synthesis of NPs [17]. So, in the present study, an emulsion solvent evaporation method was applied with physical entrapment, which depends on a limited number of chemicals.

There are two main properties of NPs—shape and size—that affect the NP carrier's behavior in the bloodstream. Particularly in small vessels and tumor capillaries, while nano-sized spherical particles can achieve efficient drug targeting [18]. In the present characterization of the designed PTX-loaded FA/PLGA NPs, size analysis showed the nano-scaled size of the particles, which improves their endocytosis [12]. SEM and TEM data showed the spherical shape of particles, which can provide the potential surface area hyperactivity. Additionally, the SEM data showed smooth surfaces, which indicate the complete drug incorporation as in previous studies [19].

Earlier studies showed that PTX-loaded PLGA NPs can achieve in vitro potential cytotoxicity that is greater than Taxol against cancer cells [20–23]. Here, we focused on CSCs' subpopulation and show that PTX-loaded FA/PLGA NPs had significant in vitro antineoplastic efficiency on primary human OCSCs compared to free PTX. The previous established primary cell line with apoptotic characteristics and chemotherapy resistance was used in this study [15]. The higher antineoplastic efficiency may be

related to the incorporation of PTX by the polymer such that it is hidden and not recognized by drug transporters on CSC membrane. Previous studies suggested that incorporation of drug by NPs can allow endocytosis and enhance intercellular drug concentration [24].

PTX-loaded PLGA NPs have been shown in many previous studies to be a successful in vivo antineoplastic system for cancer therapy [25,26]. In the present experiments, it was observed that the in vivo therapeutic and targeting efficiency of PTX might be better after loading on FA/PLGA NPs because of the higher tumor volume suppression. The higher anti-tumor efficiency of drug after incorporating on FA/PLGA NPs is related to the active targeting mechanism mediated by FA, while the interaction between FA and FR-expressed cells improves the cellular uptake of NPs as reported previously [14]. Thus, the DDS developed with FA/PLGA NPs enhanced the drug concentration in tumor cells and achieved higher therapeutic effect.

This study was supported with extra pathological evaluations of tumor tissue after treatment with PTX-loaded FA/PLGA NPs. Histopathological examination of tumors showed the effective biological influence of PTX-loaded FA/PLGA NPs through the appearance of reactive lymphoid follicles, while preclinical studies have shown that PTX reduces the interstitial fluid pressure [27]. Reactive follicular hyperplasia indicates the greater anti-tumor effect of PTX after loading on FA/PLGA NPs. Furthermore, higher efficiency of FA/PLGA NPs as carrier for PTX appears through the immunohistochemically observed higher expression of caspase-3 and P53 as apoptotic and tumor suppressor proteins. We explain these results with the fact that caspase-3 and P53 proteins enhance apoptosis in many pathways [28,29]. Moreover, molecular analysis showed the higher expression of chemo-resistant genes (*MDR1* and *ABCG2*) in the case of free PTX-based treatment compared to PTX-loaded FA/PLGA NPs. Reduction of chemo-resistant genes in the case of FA/PLGA NPs is explained by the incorporation of the chemo-drug by FA/PLGA NPs so that it cannot be detected by drug transporters on cancer cell membrane and therefore does not allow endocytosis [30].

We propose that FA/PLGA NPs are a safe carrier for PTX based on the healthy body weight of treated mice and the normal histopathological analysis of other body organs, which is in line with previous studies [31]. Minimizing the toxicity and side effects of PTX proved the active targeting efficiency of FA/PLGA NPs.

Efficient and specific CSCs targeting is considered as a key goal for cancer therapy. Nanoscale DDS based on polymeric NPs provide many unique advantages that are not available with other traditional cancer therapies [18]. Collectively, the results of this study suggest that FA/PLGA NPs can be used as DDS for PTX to improve its antineoplastic effect against OCSCs while minimizing systemic side effects.

Studying the heterogeneity of cancer biology, particularly CSCs' subpopulations, may help to understand how to achieve real therapy. Designing drug-loaded NPs should be supported by studying the interaction between NPs and the cancer microenvironment in order to improve the relationship between promising in vitro results and disappointing results in human and clinical trials.

4. Materials and Methods

4.1. Chemicals

PLGA (75%:25%, molecular weight: 8.8 KDa), PTX (molecular weight: 853.9 g/mol), poly-vinyl alcohol (PVA, molecular weight: 30 KDa) and FA were purchased from Fermentas Thermo Fisher Scientific, Waltham, MA, USA. 3-(4,5-Dimethylthiazol-2-yl)-(2,5-diphenyl tetrazolium bromide) (MTT) was purchased from Miltenyi Biotec Inc., Auburn, CA, USA. Deionized water was used throughout the experiments.

4.2. Synthesis of PTX-Loaded FA/PLGA NPs

PTX-loaded FA/PLGA NPs were prepared by an emulsion solvent evaporation technique (physical entrapment) [32,33]. One gram of PLGA was dissolved in 40 mL acetone, and PTX (20 mg)

was subsequently added. The oil solution was then stirred for 10 min at room temperature (drug: polymer ratio = 1:50). Five milligrams of FA were added into 80 mL of PVA (0.05%) solution and homogenized for 15 min at 80 °C. Oil phase was emulsified in water phase (O/W emulsion) using a probe sonicator (VCX 130, Sonic and Materials, Newtown, CT, USA), 60 watt, cycles of 5 s sonication followed by 1 s of pauses, total time 8 min (oil phase:water phase ratio = 1:2). Solvent was evaporated by continuous stirring for two hours and then centrifuged for 20 min at $33,540 \times g$ at 4 °C. The supernatant was subsequently discarded and the pellet was freeze dried for 48 hours (Free Zone 2.5-L freeze-dry system; Labconco, Kansas City, MO, USA).

4.3. Characterization of NPs

4.3.1. Particle Size Measurement

Freeze-dried NPs were dispersed in distilled water (1 mg/mL). NPs' mean particle size was detected with photon correlation spectroscopy using a Zetasizer Nano ZS90 (Malvern Instruments, Malvern, UK).

4.3.2. Surface Morphology

The surface morphology of FA/PLGA NPs was determined with scanning electron microscopy (SEM) Philips XL 30 (Philips, The Netherlands) and transmission electron microscopy (TEM) (CM-10; Philips). In SEM, a powder sample of freeze-dried NPs was stacked onto metallic stud with conductive tapes. The sample was coated with 20 nm gold layer using a sputter coater for SEM. In TEM, a sample of lyophilized NPs was suspended in distilled water and mixed by sonication for 2 min. A drop of the NPs suspension was placed on a grid and dried at room temperature.

4.3.3. Drug Loading and Encapsulation Efficiency

Prepared PTX-loaded FA/PLGA NPs were dispersed in distilled water (20 mg/mL) and placed on a shaker for 24 h. The solution was then centrifuged and PTX content in the supernatant was measured with high-performance liquid chromatography (HPLC) (Agilent 1200 Compact LC; Agilent Technologies, Santa Clara, CA, USA). Drug loading and encapsulation efficiency were calculated using Equations (1) and (2) [34]:

$$\text{Drug loading (\%)} = \text{Weight of paclitaxel in sample} / \text{Total amount of sample} \times 100 \quad (1)$$

$$\text{Encapsulation efficiency (\%)} = \text{Actual paclitaxel loading} / \text{Theoretical paclitaxel loading} \times 100 \quad (2)$$

4.4. Cell Line

Primary human ovarian cancer stem cell lines CD44+ and CD24– were established at Medical Experimental Research Center (MERC, Mansoura, Egypt). The cell lines were cultivated in Dulbecco's modified Eagle's medium (DMEM), supplemented with 10% fetal bovine serum, 1% L-glutamine and 1% penicillin-streptomycin, which were purchased from Miltenyi Biotec Inc., and incubated at 37 °C, 5% CO₂.

4.5. In Vitro Cytotoxicity of PTX-Loaded FA/PLGA NPs

The cytotoxicity of PTX-loaded FA/PLGA NPs was studied on OCSCs using the MTT assay. Briefly, OCSCs were seeded in 96-well plates at a density of 1×10^4 viable cells/well and incubated for 24 h to allow cell attachment. The medium was replaced with 100 µL of the formulation at concentrations of 0.5–10 nM after 24 h. For free PTX, a stock concentration was prepared in DMSO (1 mg/mL). The diluent for fixing the needed different concentrations for free PTX was serum-free media. Old media was removed and well plates were washed with 100 µL of phosphate-buffered saline (PBS). Seventy-five µL MTT (1 mg/mL PBS) was added to each well after 24 h and the culture

medium containing MTT solution was removed after 3–4 h incubation. The formazan crystals were dissolved in 100 μ L DMSO and read at 570 nm with a microplate reader. Cytotoxicity testing was done in triplicates.

4.6. Animals

Athymic homozygous female nude mice were purchased from Swiss Nu/Nu, Charles River Laboratories, Paris, France and were 5–6 weeks old and weighed between 16 and 18 g. All experimental animals were housed (three per cage) in polycarbonate cages and kept on a 12 h light/dark cycle under specific pathogen-free conditions. Food and water were given ad libitum. Approval for housing and breeding was obtained from the Mansoura Medical Research Ethics Committee of the University of Mansoura (protocol number: RZOO1; approval date: 26 January 2017).

4.7. In Vivo Targeting Efficiency of PTX-Loaded FA/PLGA NPs

4.7.1. Tumor Induction (Xenograft Method)

Tumors were induced in mice by subcutaneous injection of about 10^6 human OCSCs dispersed in 100 μ L DMEM in the right and left flanks on the dorsal side. Tumor volumes were determined every day by measuring both diameters and calculated using Equation (3) [35]:

$$\text{Tumor volume (mm}^3\text{)} = 1/2(\text{Long diameter} \times \text{Short diameter}^2) \quad (3)$$

When tumors reached a volume of about 1125 mm³, treatment was begun, as described next.

4.7.2. Experimental Groups

Mice were divided into four groups and tumor size was optimized between groups, three mice in each group as follows: first group injected with 200 μ L PBS (control), second group injected with plain NPs (drug-free NPs) dispersed in 200 μ L PBS, third group injected with 10 mg/kg body weight free PTX, and fourth group injected with 10 mg/kg body weight PTX-loaded NPs dispersed in 200 μ L PBS. A single IV dose was administered through the tail vein.

4.7.3. Evaluation of Tumor Volume and Body Weight Change

The long and short diameters of tumors were measured daily with calipers after treatment. Tumor volume was calculated with Equation (3). Additionally, body weights were measured daily for all mice after treatment.

4.7.4. Histopathological Examination

At the end of treatment, the mice were euthanized. Tumor and other organs (kidney, liver, pancreas, ovary, uterus, oviduct, and intestine) were harvested from each mouse, fixed in formalin, embedded in paraffin, and stained by hematoxylin and eosin (H and E) stain. Sections were microscopically examined.

4.7.5. Immunohistochemical Investigation

Slices 5 μ m thick were cut from the formalin-fixed, paraffin-embedded tumor tissue blocks and the expressions of caspase-3 and P53 proteins were detected with immunohistochemical staining. The primary antibodies used were caspase-3 (Diagnostic Biosystems, Pleasanton, CA, USA) and P53 (Genemed Synthesis, San Antonio, TX, USA). An immunohistochemistry staining kit from Power-Stain HRP (Genemed Synthesis) was used for further staining. The chromogen used was diaminobenzidine (DAB), which produces a brown color at the site of reaction. Finally, sections were counterstained with hematoxylin and mounted.

4.8. Gene Expression Analysis

Real-time qPCR (RT-qPCR) analysis was applied, starting with RNA that was isolated from the freshly harvested tumors using the TRIzol Reagent and purified with GeneJET™ RNA Purification Kit (Fermentas Thermo Fisher Scientific). One µg of RNA from each sample was applied for reverse transcription using the Maxima® First Strand cDNA Synthesis Kit (Fermentas Thermo Fisher Scientific). RT qPCR was done with the Maxima® SYBR Green qPCR Master Mix (Fermentas Thermo Fisher Scientific). Reactions were done in a 20 µL volume with 20 pmol primers. The primers for the *ABCG2*, *MDR1*, *Caspase3*, *Caspase9*, and *TP53* genes are listed in the Supplementary (Table S1), with GAPDH as a control. qPCR was performed with a RT PCR detection system (Agilent Technologies) with an initial denaturation at 95 °C for 10 min, followed by 40 cycles for 15 s at 95 °C, 30 s at melting temperature –5 °C, and 30 s at 72 °C. Specificity was detected with melting curve analysis. qPCR products were electrophoresed on 2% agarose gels. The Ct values of samples were used in the qPCR data analysis. Quantitative analysis was applied to evaluate the chemo-resistant, apoptotic and tumor suppressor genes' fold change between both forms of PTX (free PTX and PTX-loaded FA/PLGA NPs).

4.9. Statistical Analysis

IC₅₀ values were determined with GraphPad Prism 5 software (GraphPad, San Diego, CA, USA) and Excel. The collected data of tumor volumes and body weights were organized and statistically analyzed using one-way ANOVA, followed by the Tukey post-hoc test with $p < 0.05$. Genes' fold change was calculated and analyzed with the $2^{-\Delta\Delta Ct}$ method from RT-qPCR experiments [36].

5. Conclusions

This study concludes that DDS based on polymeric NPs can provide the specific characteristics to overcome the chemo-resistant property of CSCs in ovarian cancer by enhancing in vitro cytotoxic efficacy of chemo-drug and improving its in vivo anti-tumor and targeting efficiency. These findings indicate that PTX-loaded FA/PLGA NPs are a successful and safe therapeutic design against human OCSCs in in vitro and in vivo mouse models.

Supplementary Materials: Supplementary materials can be found at www.mdpi.com/1422-0067/18/4/813/s1.

Acknowledgments: This work was supported by King Saud University, Deanship of Scientific Research, College of Science Research Center. We thank "Zewail City" and "MERC" of Mansoura Faculty of Medicine for their support. A special thank you goes to Yomna Khater, Veterinarian at MERC, for her support. We appreciate the excellent editorial assistance of Kelly Keating (The Pharmaceutical Research Institute, Rensselaer, NY USA).

Author Contributions: Amoura Abou-ElNaga directed the experiments from conception to production and revised the manuscript. Ghada Mutawa performed the experiments, analyzed the data, wrote the manuscript and contributed chemicals. Ibrahim M. El-Sherbiny designed and managed the experiments of the synthesis and characterization of nanoparticles. Hassan Abd-ElGhaffar contributed the cell lines and experimental animals. Ahmed A. Allam and Jamaan Ajarem contributed reagents, materials, and analysis tools. Shaker A. Mousa conceived the main idea of the research, analyzed data, and revised the manuscript.

Conflicts of Interest: The authors declare no conflict of interest.

Abbreviations

DDS	Drug delivery system
OCSC	Ovarian cancer stem cell
PTX	Paclitaxel
PLGA	Poly(lactic-co-glycolic acid)
NP	Nanoparticle
FA	Folic acid
FR	Folic receptor
IC ₅₀	Half maximal inhibitory concentration

References

1. Donninger, H.; Bonome, T.; Radonovich, M.; Pise-Masison, C.A.; Brady, J.; Shih, J.H.; Barrett, J.C.; Birrer, M.J. Whole genome expression profiling of advance stage papillary serous ovarian cancer reveals activated pathways. *Oncogene* **2004**, *23*, 8065–8077. [[CrossRef](#)] [[PubMed](#)]
2. Meng, E.; Long, B.; Sullivan, P.; McClellan, S.; Finan, M.A.; Reed, E.; Shevde, L.; Rocconi, R.P. CD44+/CD24– ovarian cancer cells demonstrate cancer stem cell properties and correlate to survival. *Clin. Exp. Metastasis* **2012**, *29*, 939–948. [[CrossRef](#)] [[PubMed](#)]
3. Lv, W.; Cheng, L.; Li, B. Development and evaluation of a novel TPGS-mediated paclitaxel-loaded PLGA-mPEG nanoparticle for the treatment of ovarian cancer. *Chem. Pharm. Bull.* **2015**, *63*, 68–74. [[CrossRef](#)] [[PubMed](#)]
4. Walters Haygood, C.L.; Arend, R.C.; Straughn, J.M.; Buchsbaum, D.J. Ovarian cancer stem cells: Can targeted therapy lead to improved progression-free survival? *World J. Stem Cells* **2014**, *6*, 441–447. [[CrossRef](#)] [[PubMed](#)]
5. Blagosklonny, M.V. Target for cancer therapy: Proliferating cells or stem cells. *Leukemia* **2006**, *20*, 385–391. [[CrossRef](#)] [[PubMed](#)]
6. Lou, H.; Dean, M. Targeted therapy for cancer stem cells: The patched pathway and ABC transporters. *Oncogene* **2007**, *26*, 1357–1360. [[CrossRef](#)] [[PubMed](#)]
7. Kolhe, S.; Parikh, K. Application of nanotechnology in cancer: A review. *Int. J. Bioinform. Res. Appl.* **2012**, *8*, 112–125. [[CrossRef](#)] [[PubMed](#)]
8. Bae, K.H.; Chung, H.J.; Park, T.G. Nanomaterials for cancer therapy and imaging. *Mol. Cells* **2011**, *31*, 295–302. [[CrossRef](#)] [[PubMed](#)]
9. Feng, S.S.; Chien, S. Chemotherapeutic engineering: Application and further development of chemical engineering principles for chemotherapy of cancer and other diseases. *Chem. Eng. Sci.* **2003**, *58*, 4087–4114. [[CrossRef](#)]
10. Kumari, A.; Yadav, S.K.; Yadav, S.C. Biodegradable polymeric nanoparticles based drug delivery systems. *Colloids Surf. B* **2010**, *75*, 1–18. [[CrossRef](#)] [[PubMed](#)]
11. Danhier, F.; Ansorena, E.; Silva, J.M.; Coco, R.; Le Breton, A.; Preat, V. PLGA-based nanoparticles: An overview of biomedical applications. *J. Control. Release* **2012**, *161*, 505–522. [[CrossRef](#)] [[PubMed](#)]
12. Bertrand, N.; Wu, J.; Xu, X.; Kamaly, N.; Farokhzad, O.C. Cancer nanotechnology: The impact of passive and active targeting in the era of modern cancer biology. *Adv. Drug Deliv. Rev.* **2014**, *66*, 2–25. [[CrossRef](#)] [[PubMed](#)]
13. Kirpotin, D.B.; Drummond, D.C.; Shao, Y.; Shalaby, M.R.; Hong, K.; Nielsen, U.B.; Marks, J.D.; Benz, C.C.; Park, J.W. Antibody targeting of long-circulating lipidic nanoparticles does not increase tumor localization but does increase internalization in animal models. *Cancer Res.* **2006**, *66*, 6732–6740. [[CrossRef](#)] [[PubMed](#)]
14. Stella, B.; Marsaud, V.; Arpicco, S.; Geraud, G.; Cattel, L.; Couvreur, P.; Renoir, J.M. Biological characterization of folic acid-conjugated poly(H₂NPEGCA-co-HDCA) nanoparticles in cellular models. *J. Drug Target* **2007**, *15*, 146–153. [[CrossRef](#)] [[PubMed](#)]
15. Abouelnaga, A.; Mutawa, G.A.; Abdelghaffar, H.; Sobh, M.; Hamed, S.; Mousa, S.A. Establishment and characterization of primary human ovarian cancer stem cell line (CD44+ve). *J. Cancer Res. Updates* **2016**, *5*, 59–66.
16. Zheng, X.; Cui, D.; Xu, S.; Brabant, G.; Derwahl, M. Doxorubicin fails to eradicate cancer stem cells derived from anaplastic thyroid carcinoma cells: Characterization of resistant cells. *Int. J. Oncol.* **2010**, *37*, 307–315. [[PubMed](#)]
17. De Jong, W.H.; Borm, P.J. Drug delivery and nanoparticles: Applications and hazards. *Int. J. Nanomed.* **2008**, *3*, 133–149. [[CrossRef](#)]
18. Calderera-Moore, M.; Guimard, N.; Shi, L.; Roy, K. Designer nanoparticles: Incorporating size, shape and triggered release into nanoscale drug carriers. *Expert Opin. Drug Deliv.* **2010**, *7*, 479–495. [[CrossRef](#)] [[PubMed](#)]
19. Mathew, A.; Fukuda, T.; Nagaoka, Y.; Hasumura, T.; Morimoto, H.; Yoshida, Y.; Maekawa, T.; Venugopal, K.; Kumar, D.S. Curcumin loaded-PLGA nanoparticles conjugated with tet-1 peptide for potential use in alzheimer's disease. *PLoS ONE* **2012**, *7*, e32616. [[CrossRef](#)] [[PubMed](#)]

20. Lopez-Gasco, P.; Iglesias, I.; Benedi, J.; Lozano, R.; Teijon, J.M.; Blanco, M.D. Paclitaxel-loaded polyester nanoparticles prepared by spray-drying technology: In vitro bioactivity evaluation. *J. Microencapsul.* **2011**, *28*, 417–429. [[CrossRef](#)] [[PubMed](#)]
21. Vicari, L.; Musumeci, T.; Giannone, I.; Adamo, L.; Conticello, C.; De Maria, R.; Pignatello, R.; Puglisi, G.; Gulisano, M. Paclitaxel loading in PLGA nanospheres affected the in vitro drug cell accumulation and antiproliferative activity. *BMC Cancer* **2008**, *8*, 212. [[CrossRef](#)] [[PubMed](#)]
22. Danhier, F.; Lecouturier, N.; Vroman, B.; Jerome, C.; Marchand-Brynaert, J.; Feron, O.; Preat, V. Paclitaxel-loaded pegylated PLGA-based nanoparticles: In vitro and in vivo evaluation. *J. Control. Release* **2009**, *133*, 11–17. [[CrossRef](#)] [[PubMed](#)]
23. Fonseca, C.; Simoes, S.; Gaspar, R. Paclitaxel-loaded PLGA nanoparticles: Preparation, physicochemical characterization and in vitro anti-tumoral activity. *J. Control. Release* **2002**, *83*, 273–286. [[CrossRef](#)]
24. Sneh-Edri, H.; Likhtenshtein, D.; Stepensky, D. Intracellular targeting of PLGA nanoparticles encapsulating antigenic peptide to the endoplasmic reticulum of dendritic cells and its effect on antigen cross-presentation in vitro. *Mol. Pharm.* **2011**, *8*, 1266–1275. [[CrossRef](#)] [[PubMed](#)]
25. Liu, P.; Situ, J.Q.; Li, W.S.; Shan, C.L.; You, J.; Yuan, H.; Hu, F.Q.; Du, Y.Z. High tolerated paclitaxel nano-formulation delivered by poly (lactic-co-glycolic acid)-g-dextran micelles to efficient cancer therapy. *Nanomedicine* **2015**, *11*, 855–866. [[CrossRef](#)] [[PubMed](#)]
26. Noori Koopaei, M.; Khoshayand, M.R.; Mostafavi, S.H.; Amini, M.; Khorramizadeh, M.R.; Jeddi Tehrani, M.; Atyabi, F.; Dinarvand, R. Docetaxel loaded PEG-PLGA nanoparticles: Optimized drug loading, in vitro cytotoxicity and in vivo antitumor effect. *Iran. J. Pharm. Res.* **2014**, *13*, 819–833. [[PubMed](#)]
27. Taghian, A.G.; Abi-Raad, R.; Assaad, S.I.; Casty, A.; Ancukiewicz, M.; Yeh, E.; Molokhia, P.; Attia, K.; Sullivan, T.; Kuter, I.; et al. Paclitaxel decreases the interstitial fluid pressure and improves oxygenation in breast cancers in patients treated with neoadjuvant chemotherapy: Clinical implications. *J. Clin. Oncol.* **2005**, *23*, 1951–1961. [[CrossRef](#)] [[PubMed](#)]
28. Lakshman, M.; Subramaniam, V.; Rubenthiran, U.; Jothy, S. CD44 promotes resistance to apoptosis in human colon cancer cells. *Exp. Mol. Pathol.* **2004**, *77*, 18–25. [[CrossRef](#)] [[PubMed](#)]
29. Godar, S.; Ince, T.A.; Bell, G.W.; Feldser, D.; Donaher, J.L.; Bergh, J.; Liu, A.; Miu, K.; Watnick, R.S.; Reinhardt, F.; et al. Growth-inhibitory and tumor-suppressive functions of p53 depend on its repression of CD44 expression. *Cell* **2008**, *134*, 62–73. [[CrossRef](#)] [[PubMed](#)]
30. Xue, X.; Liang, X.J. Overcoming drug efflux-based multidrug resistance in cancer with nanotechnology. *Chin. J. Cancer* **2012**, *31*, 100–109. [[CrossRef](#)] [[PubMed](#)]
31. Zhao, T.; Chen, H.; Dong, Y.; Zhang, J.; Huang, H.; Zhu, J.; Zhang, W. Paclitaxel-loaded poly(glycolide-co-epsilon-caprolactone)-*b*-D- α -tocopheryl polyethylene glycol 2000 succinate nanoparticles for lung cancer therapy. *Int. J. Nanomed.* **2013**, *8*, 1947–1957. [[PubMed](#)]
32. Boddu, S.H.S.; Vaishya, R.; Jwala, J.; Vadlapudi, A.; Pal, D.; Mitra, A.K. Preparation and characterization of folate conjugated nanoparticles of doxorubicin using Plga-Peg-Fol polymer. *Med. Chem.* **2012**, *2*, 68–75. [[CrossRef](#)]
33. Katsikogianni, G.; Avgoustakis, K. Poly(lactide-co-glycolide)-methoxy-poly(ethylene glycol) nanoparticles: Drug loading and release properties. *J. Nanosci. Nanotechnol.* **2006**, *6*, 3080–3086. [[CrossRef](#)] [[PubMed](#)]
34. Kashi, T.S.; Eskandarion, S.; Esfandyari-Manesh, M.; Marashi, S.M.; Samadi, N.; Fatemi, S.M.; Atyabi, F.; Eshraghi, S.; Dinarvand, R. Improved drug loading and antibacterial activity of minocycline-loaded PLGA nanoparticles prepared by solid/oil/water ion pairing method. *Int. J. Nanomed.* **2012**, *7*, 221–234. [[PubMed](#)]
35. Jensen, M.M.; Jørgensen, J.T.; Binderup, T.; Kjær, A. Tumor volume in subcutaneous mouse xenografts measured by microCT is more accurate and reproducible than determined by ^{18}F -FDG-microPET or external caliper. *BMC Med. Imaging* **2008**, *8*, 16. [[CrossRef](#)] [[PubMed](#)]
36. Livak, K.J.; Schmittgen, T.D. Analysis of relative gene expression data using real-time quantitative PCR and the $2^{-\Delta\Delta\text{CT}}$ method. *Methods* **2001**, *25*, 402–408. [[CrossRef](#)] [[PubMed](#)]

